Mechanism and Machine Theory 46 (2011) 534–543

Contents lists available at ScienceDirect

Mechanism and Machine Theory

journal homepage: www.elsevier.com/locate/mechmt

Tooth flank, undercutting and tooth pointing of spherical gears

Li-Chi Chao [a], Chung-Biau Tsay [b,*]

[a] Department of Mechanical Engineering, National Chiao Tung University, Hsinchu 30010, Taiwan
[b] Department of Mechanical Engineering, Minghsin University of Science and Technology, Hsinchu 30401, Taiwan

ARTICLE INFO

Article history:
Received 7 January 2009
Received in revised form 2 November 2010
Accepted 16 November 2010
Available online 23 December 2010

Keywords:
Spherical gear
Profile-shifting
Tooth undercutting
Tooth pointing
Tooth profile deviation

ABSTRACT

By the developed mathematical model of spherical gears from literature [16], conditions of tooth undercutting of spherical gears with convex and concave teeth and tooth pointing conditions of the proposed concave spherical gear are derived. Besides, tooth flank profile deviations, limit curves of tooth undercutting and the beginning points of tooth undercutting and tooth pointing of the proposed spherical gear can be obtained by applying the spherical gear tooth mathematical model and the developed computer simulation programs, as illustrated by five numerical examples.

1. Introduction

A convex and concave spherical gear can be considered as a spur gear with continuous positive and negative profile-shiftings in a quadric form beginning from both ends of the tooth face width to the middle section. Therefore, tooth undercutting easily occurs on the active tooth flank near both ends of the tooth face width of a convex spherical gear, while tooth pointing easily occurs on the tooth top near both ends of the tooth face width of a concave spherical gear. It is well known that tooth undercutting of a gear may decrease the gear strength and contact ratio of a gear pair, while tooth pointing of a gear may get wear near the tooth top. Therefore, the conditions of tooth undercutting and pointing are important issues for gear design and manufacturing, and literatures on the topics have received considerable attention. Some researchers [1,2] investigated the evolution in design theory and gearing applications. In the pioneer work, Litvin [3], and Litvin and Fuentes [4] proposed a method for investigation on the conditions of tooth pointing and tooth undercutting by considering the relative velocity and equation of meshing. Chang et al. [5] developed a mathematical model and investigated the undercutting condition of elliptical gears generated by rack cutters. Liu and Tsay [6] studied the tooth undercutting of beveloid gears, and proposed two practicable methods to avoid the tooth undercutting on active tooth flanks. Chen et al. [7] studied the mathematical model and tooth undercutting of the modified helical gears with a smaller number of teeth. The mathematical model and undercutting analysis of cylindrical gears with curvilinear shaped teeth were investigated by Tseng and Tsay [8]. The tooth profile deviation of cylindrical gears with curvilinear shaped teeth was also studied by Tseng and Tsay [9]. Furthermore, Yang [10,11] proposed a ring-involute-teeth spherical gear with double degrees of freedom. Yang [12] applied the spherical gear with double degrees of freedom to the elbow mechanism. Tsai and Jehng [13] applied a rapid prototyping to manufacture a spherical gear with skew axes. However, both spherical gears investigated by Yang [10–12] and Tsai and Jehng [13] are different from that proposed in this study either in generation mechanism, teeth profiles, transmission characteristics or meshing model of gear set. Moreover, Novikov [14] proposed a helical gear with circular tooth profile, and it is the so-called Novikov gear. However, the spherical gear proposed here, having concave and convex tooth shapes along its tooth width direction, is different from that of the Novikov gear.

* Corresponding author. Tel.: +886 3 5719991.
E-mail address: cbtsay@mail.nctu.edu.tw (C.-B. Tsay).

0094-114X/$ – see front matter © 2010 Elsevier Ltd. All rights reserved.
doi:10.1016/j.mechmachtheory.2010.11.007

Nomenclature

a, b	Design parameter of rack cutter ($i=F, P$) (Fig. 2 and Table 1)
ℓ_i	Profile parameter of rack cutter ($i=F, P$)
m_n	Normal module (Table 1)
N_j	Number of teeth of spherical gear ($j=1, 2$) (Table 1)
r_{tl}	Radius of tooth top circle (Fig. 2 and Eq. (12))
R_j	Spherical radius ($j=1, 2$) (Fig. 1 and Table 1)
$\mathbf{R}_f^{(i)}$	Position vector of surface Σ_i ($i=F, P$) expressed in coordinate system S_f (Eq. (5))
$\mathbf{R}_j$	Position vector of surface Σ_j ($j=1, 2$) expressed in coordinate system S_j (Eqs. (1), (2) and (12))
S_f (X_f, Y_f, Z_f)	Cartesian coordinate system f with three mutual perpendicular axes X_f, Y_f and Z_f
t_{tl}	Tooth thickness of tooth topland (Fig. 2)
$\mathbf{T}$	Tangent vector to the generated tooth flank
$V_x^{(ij)}, V_y^{(ij)}, V_z^{(ij)}$	X, Y and Z components of relative velocity $\mathbf{V}^{(ij)}$, between rack cutter i ($i=F, P$) and spherical gear j ($j=1, 2$) (Eqs. (6)–(9))
$\mathbf{V}^{(ij)}$	Relative velocity (sliding velocity) of a point of rack cutter surface Σ_i ($i=F, P$) with respect to the same point of the generated gear surface Σ_j ($j=1, 2$)
$\mathbf{V}_r^{(j)}$	Relative velocity of a point of surface Σ_j ($j=1, 2$) in its relative motion over the same surface Σ_j ($j=1, 2$)
W	Face width of the spherical gear (Figs. 1, 4, 5 and Table 1)
α_n	Normal pressure angle (Table 1)
θ_j	Spherical angle of the spherical gear j ($j=1, 2$)
ω_h, ω_j	Angular velocities of hob cutter h and generated gear j ($j=1, 2$) (Fig. 1)

Table 1
Major design parameters of external spherical and spur gears.

Type of gears	Convex tooth	Concave tooth	Spur
Normal module m_n (mm/teeth)	2	2	2
Design parameter a (mm)	2	2	2
Design parameter b (mm)	3.1416	3.1416	3.1416
Example 1			
Normal pressure angle α_n (deg.)	20	20	20
Number of teeth N_j	33	33	33
Face width W (mm)	15	15	15
Spherical gear radius R_j (mm)	33	33	–
Max. spherical angle θ_j (deg.)	±13.137	±13.137	–
Example 2			
Normal pressure angle α_n (deg.)	14.5	14.5	–
Number of teeth N_j	33	28	–
Face width W (mm)	15	15	–
Spherical gear radius R_j (mm)	33	33	–
Max. spherical angle θ_j (deg.)	±13.137	±15.537	–
Example 3			
Normal pressure angle α_n (deg.)	14.5	14.5	–
Number of teeth N_j	23/31/37/43	29/33/37/41	–
Face width W (mm)	15	15	–
Spherical gear radius R_j (mm)	23/31/37/43	29/33/37/41	–
Max. spherical angle θ_j (deg.)	±19.031/±14.001/±11.695/±10.045	±14.988/±13.137/±11.695/±10.54	–
Example 4			
Normal pressure angle α_n (deg.)	14.5/20/25	–	–
Number of teeth N_j	18–36	–	–
Spherical gear radius R_j (mm)	18–36		
Example 5			
Normal pressure angle α_n (deg.)	–	14.5/20/25	–
Number of teeth N_2	–	15–35	–
Spherical gear radius R_2 (mm)	–	15–35	–

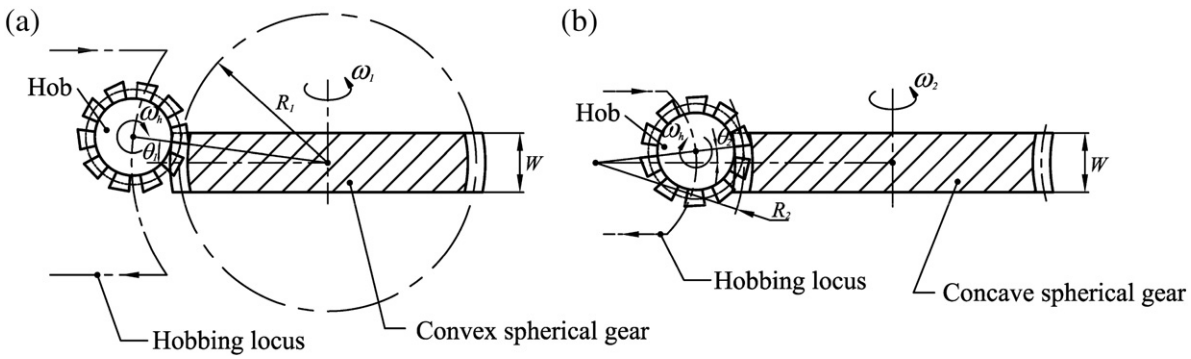

Fig. 1. Hobbing locus for spherical gears with (a) convex teeth and (b) concave teeth.

Since the spherical gear is hobbed by a hob cutter, the convex and concave spherical gears can be considered as hobbing a spur gear with its hobbing path of continuous positive-direction or negative-direction profile-shiftings in a quadric form, beginning from both sides of the tooth face width to its middle section, respectively [15,16]. Where the positive-direction profile-shifting is set as the direction outward the generated gear, whereas the negative-direction profile-shifting is set as the direction inward the generated gear. Compared with the standard tooth profile of a spur gear, the tooth profiles at both ends of tooth face width of the convex spherical gear have negative profile-shifting, whereas the same profiles of the concave spherical gear have positive profile-shifting. Therefore, the occurrence of tooth undercuttings on both ends of the face width is easier than that at the middle section for a convex spherical gear, whereas the inverse situation exists for the concave spherical gear tooth flanks.

Different from the conventional spur gear set, the spherical gear set allows variable shaft angles and larger axial misalignments without gear interference in meshing. Besides, the spherical gear allows assembly errors of axial-misalignments, and its bearing contact still located on the middle region of the tooth width. The spur gear and conical gear drives are sensitive to axial-misalignments since these may result in edge contact of the gear drive. Moreover, the hobbing path of a spherical gear is generated by hobbing a cylinder with a quadric form of continuous profile-shifting (i.e. an arc) along the gear rotation axis instead of a straight line for conventional spur gear's generation.

Further, based on the spherical gear's mathematical model [16] and theory of gearing, the tooth undercutting and tooth pointing of the proposed spherical gear, and the tooth flank profile deviations of the spur and proposed spherical gears are investigated and demonstrated by five numerical examples. Moreover, the limit curves and the beginning points of tooth undercutting and pointing are also studied.

2. Mathematical model representations of spherical gears developed in Ref. [16]

In this section, two hobbing loci of a hob cutter are considered to simulate the hobbing process for spherical gears with convex teeth and concave teeth, as shown in Fig. 1. According to the theory of gearing and the gear hobbing mechanism, the mathematical model of spherical gears with convex and concave teeth has been developed in literature [16]. For brevity, the development of

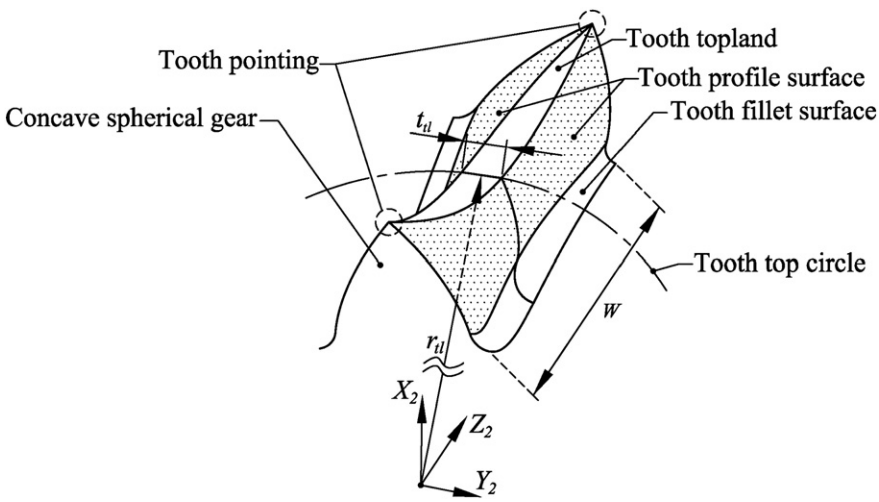

Fig. 2. Tooth pointing of concave spherical gear.

mathematical model for convex and concave spherical gears is not presented in detail here. Therefore, the locus equations of rack cutter surfaces (Σ_F and Σ_P) for convex and concave spherical gears (Σ_1 and Σ_2) can be referred to the literature [16] and attained respectively as follows [16]:

$$\mathbf{R}_1 = \begin{bmatrix} [(-a + \ell_F\cos\alpha_n + R_1)\cos\theta_1 - R_1 + r_1]\cos\phi_1 - [\mp b \mp a\tan\alpha_n \pm \ell_F\sin\alpha_n - r_1\phi_1]\sin\phi_1 \\ [(-a + \ell_F\cos\alpha_n + R_1)\cos\theta_1 - R_1 + r_1]\sin\phi_1 + [\mp b \mp a\tan\alpha_n \pm \ell_F\sin\alpha_n - r_1\phi_1]\cos\phi_1 \\ (a - \ell_F\cos\alpha_n + R_1)\sin\theta_1 \end{bmatrix}, \tag{1}$$

and

$$\mathbf{R}_2 = \begin{bmatrix} [(-a + \ell_P\cos\alpha_n + R_2)\cos\theta_2 - R_2 - r_2]\cos\phi_2 + [\mp b \mp a\tan\alpha_n \pm \ell_P\sin\alpha_n - r_2\phi_2]\sin\phi_2 \\ -[(-a + \ell_P\cos\alpha_n + R_2)\cos\theta_2 - R_2 - r_2]\sin\phi_2 + [\mp b \mp a\tan\alpha_n \pm \ell_P\sin\alpha_n - r_2\phi_2]\cos\phi_2 \\ (a - \ell_P\cos\alpha_n + R_2)\sin\theta_2 \end{bmatrix}, \tag{2}$$

where symbols R_1 and R_2 represent the spherical radii of a convex tooth and a concave tooth, respectively, and symbols θ_1 and θ_2 denote the spherical angles of a convex tooth and a concave tooth, measured from the central section of the spherical gears to the position of hob cutter's normal section at every rotation instant, in the gears hobbing process, respectively. Moreover, symbol α_n indicates the pressure angle of the spherical gears. Parameters ℓ_i ($i = F, P$) and θ_j ($j = 1, 2$) are the surface coordinates of the rack cutter surfaces, respectively, where, superscripts $i = F$ corresponds to $j = 1$ while $i = P$ corresponds to $j = 2$ since rack cutter Σ_F generates gear Σ_1 and rack cutter Σ_P generates gear Σ_2.

Variant equations of meshing for the convex and concave spherical gears can be rewritten in terms of the design parameters of the gears by applying the methods from literature [16] as

$$\begin{aligned} f\left(\ell_i, \theta_j, \phi_j\right) = {} & \pm\left(a - \ell_i\cos\alpha_n + R_j\right)\left(r_j\phi_j \pm b \pm a\tan\alpha_n \mp \ell_i\sin\alpha_n\right)\cos\theta_j\sin\alpha_n \\ & + \left(a - \ell_i\cos\alpha_n + R_j\cos 2\theta_j\right)\left[\left(a - \ell_i\cos\alpha_n - R_j\right)\cos\theta_j + R_j\right]\cos\alpha_n = 0, \end{aligned} \tag{3}$$

where, superscripts $i = F$ corresponds to $j = 1$ while $i = P$ corresponds to $j = 2$ since rack cutter Σ_F generates gear Σ_1 and rack cutter Σ_P generates gear Σ_2. It is noted that the equation is in the quadric form with continuous profile-shifting (i.e. spherical radius R_j shown in Fig. 3 of the literature [16]), as shown in Eq. (3). If the spherical radius R_j ($j = 1, 2$) approaches to infinite (i.e. hobbing with a straight path), the spherical gear angle θ_j ($j = 1, 2$) will tend to zero. Therefore, the equation of meshing of the convex and concave spherical gears becomes the same as that of the spur gear. Moreover, the upper and lower signs expressed in Eqs. (1)–(3) represent the left and right sides of the rack cutter surfaces, respectively. The mathematical models of the spherical gears with convex teeth and concave teeth can be determined by simultaneously considering Eqs. (1) and (3) ($i = F$ and $j = 1$), and Eqs. (2) and (3) ($i = P$ and $j = 2$), respectively.

3. Tooth undercutting and pointing analyses

3.1. Tooth undercutting analysis

Mathematically, the phenomenon of tooth undercutting is the appearance of singular points on the active tooth flank. If the active tooth flank is a regular surface, it means that there is no singular point on the surface. Moreover, the tooth undercutting

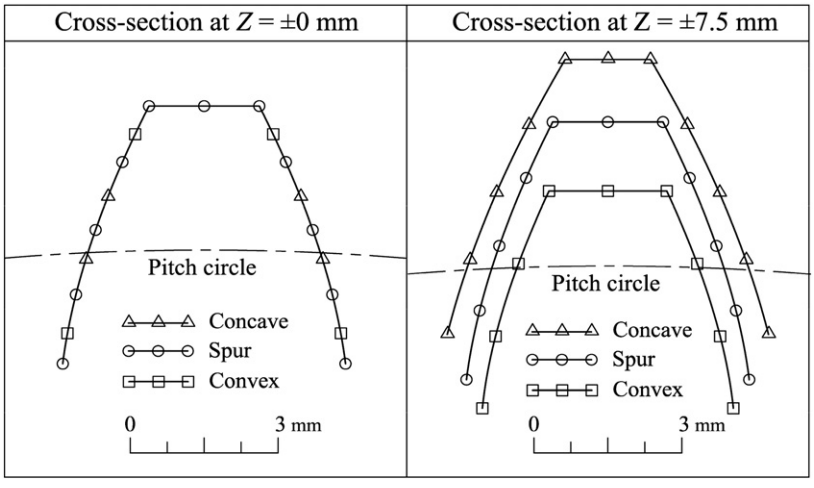

Fig. 3. Tooth flank profiles of spherical and spur gears at cross-sections $Z = 0$ mm and $Z = \pm 7.5$ mm (gear data are given in Example 1 of Table 1).

usually occurs near the tooth root. A method proposed by Litvin [3,4], which considers the relative velocity and equation of meshing between the rack cutter and generated gear, is applied in this section to determine the limit curve of tooth undercutting of the convex and concave spherical gears.

According to the general conditions of tooth undercutting [3,4], the tangent vector $\mathbf{T}$ to the generated tooth flank is collinear with its relative velocity $\mathbf{V}_r^{(j)}(j=1, 2)$. The subscript "$r$" indicates the relative velocity of a point in its relative motion over a surface. When tooth undercutting occurs, a singular point appears on the active tooth flank and the tangent vector becomes $\mathbf{T}=\mathbf{0}$ ($\mathbf{V}_r^{(j)}=\mathbf{0}$ $(j=1, 2)$). Therefore, the relative velocity at a singular point on the active tooth flank equals zero as follows:

$$\frac{\partial \mathbf{R}_f^{(i)}}{\partial \ell_i}\frac{d\ell_i}{dt} + \frac{\partial \mathbf{R}_f^{(i)}}{\partial \theta_j}\frac{d\theta_j}{dt} = -\mathbf{V}^{(ij)} \ (i = F, P \text{ and } j = 1, 2), \tag{4}$$

where symbol $\mathbf{R}_f^{(i)}(i=F, P)$ indicates the position vector of rack cutter surface expressed in the coordinate system S_f (X_f, Y_f, Z_f), while symbol $\mathbf{V}^{(ij)}$ denotes the relative velocity (sliding velocity) of a point of rack cutter surface Σ_i $(i=F, P)$ with respect to the same point of the generated gear surface Σ_j $(j=1, 2)$ (see Eq. (6) and Fig. 4 of Ref. [16]).

Differentiating Eq. (3), the equation of meshing of the rack cutter and generated convex and concave spherical gear tooth flanks, with respect to time yields

$$\frac{\partial f_j}{\partial \ell_i}\frac{d\ell_i}{dt} + \frac{\partial f_j}{\partial \theta_j}\frac{d\theta_j}{dt} = -\frac{\partial f_j}{\partial \phi_j}\frac{d\phi_j}{dt} (i = F, P \text{ and } j = 1, 2), \tag{5}$$

where superscripts $i=F$ corresponds to $j=1$ while $i=P$ corresponds to $j=2$ since rack cutter Σ_F generates gear Σ_1 and rack cutter Σ_P generates gear Σ_2.

Eq. (5) forms a system of four linear equations with two unknowns $\frac{d\ell_i}{dt}$ and $\frac{d\theta_j}{dt}$, and provides a nontrivial solution if and only if the rank of the matrix of coefficients for these equations is equal to two. Thus, the value of determinants of the third order must equal zero, and it yields the following four equality equations:

$$\Delta_1 = \begin{vmatrix} \frac{\partial X_f^{(i)}}{\partial \ell_i} & \frac{\partial X_f^{(i)}}{\partial \theta_j} & -V_x^{(ij)} \\ \frac{\partial Y_f^{(i)}}{\partial \ell_i} & \frac{\partial Y_f^{(i)}}{\partial \theta_j} & -V_y^{(ij)} \\ \frac{\partial f_j}{\partial \ell_i} & \frac{\partial f_j}{\partial \theta_j} & -\frac{\partial f_j}{\partial \phi_j}\frac{d\phi_j}{dt} \end{vmatrix} = 0, \tag{6}$$

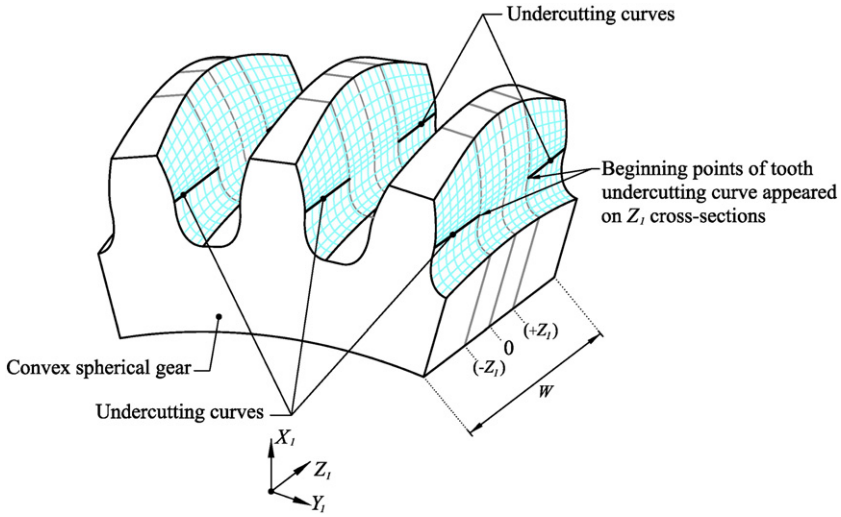

Fig. 4. Tooth undercutting of the convex spherical gear (gear data is given in Example 2 of Table 1).

$$\Delta_2 = \begin{vmatrix} \frac{\partial X_f^{(i)}}{\partial \ell_i} & \frac{\partial X_f^{(i)}}{\partial \theta_j} & -V_x^{(ij)} \\ \frac{\partial Z_f^{(i)}}{\partial \ell_i} & \frac{\partial Z_f^{(i)}}{\partial \theta_j} & -V_z^{(ij)} \\ \frac{\partial f_j}{\partial \ell_i} & \frac{\partial f_j}{\partial \theta_j} & -\frac{\partial f_j}{\partial \phi_j}\frac{d\phi_j}{dt} \end{vmatrix} = 0, \tag{7}$$

$$\Delta_3 = \begin{vmatrix} \frac{\partial Y_f^{(i)}}{\partial \ell_i} & \frac{\partial Y_f^{(i)}}{\partial \theta_j} & -V_y^{(ij)} \\ \frac{\partial Z_f^{(i)}}{\partial \ell_i} & \frac{\partial Z_f^{(i)}}{\partial \theta_j} & -V_z^{(ij)} \\ \frac{\partial f_j}{\partial \ell_i} & \frac{\partial f_j}{\partial \theta_j} & -\frac{\partial f_j}{\partial \phi_j}\frac{d\phi_j}{dt} \end{vmatrix} = 0, \tag{8}$$

and

$$\Delta_4 = \begin{vmatrix} \frac{\partial X_f^{(i)}}{\partial \ell_i} & \frac{\partial X_f^{(i)}}{\partial \theta_j} & -V_x^{(ij)} \\ \frac{\partial Y_f^{(i)}}{\partial \ell_i} & \frac{\partial Y_f^{(i)}}{\partial \theta_j} & -V_y^{(ij)} \\ \frac{\partial Z_f^{(i)}}{\partial \ell_i} & \frac{\partial Z_f^{(i)}}{\partial \theta_j} & -V_z^{(ij)} \end{vmatrix} = 0, \tag{9}$$

where Eq. (9) is identical to the equation of meshing of the spherical gears [3,4]. Eqs. (6)–(8) can be used to determine the singular points on the generated tooth flanks, and it is called the condition of tooth undercutting. Therefore, the sufficient condition of tooth undercutting can be represented by

$$F_j\left(\ell_i, \theta_j, \phi_j\right) = \Delta_1^2 + \Delta_2^2 + \Delta_3^2 = 0 (i = F, P \text{ and } j = 1, 2). \tag{10}$$

Again, superscripts $i = F$ corresponds to $j = 1$ while $i = P$ corresponds to $j = 2$ since rack cutter Σ_F generates gear Σ_1 and rack cutter Σ_P generates gear Σ_2.

3.2. Tooth pointing analysis

Different from the phenomenon of tooth undercutting, the tooth pointing of a gear occurs near the tooth topland as shown in Fig. 2. If the phenomenon of tooth pointing occurs, the tooth thickness of the gear on tooth topland becomes zero. When a mating gear pair contacts with tooth pointing and locates near the tooth top, the load capacity of the mating gear pair may get weak in the contact instant. Therefore, the tooth pointing is also an important issue for gear design and manufacturing. Moreover, the concave spherical gear can be considered as hobbing a spur gear with its hobbing path of continuous negative-direction profile-shiftings in a quadric form, beginning from both sides of the tooth face width to its middle section. Therefore, the occurrence of tooth pointing on both ends of face width is easier than that at the middle section for a concave spherical gear.

Fig. 2 illustrates the tooth pointing of a concave spherical gear occurs on the tooth topland of the gear. Symbol t_{tl} of Fig. 2 denotes the tooth thickness of the tooth topland at a Z_2 cross-section of the face width of the concave spherical gear. Since tooth pointing of a gear means that the tooth thickness of the tooth topland becomes zero ($t_{tl} = 0$ mm), the tooth pointing can also be considered as the left-side and right-side tooth flank profiles of a gear are intersected as a point at its tooth topland in Z_2 cross-section of the face width. According to the concept of tooth pointing, the condition equations of tooth pointing at the Z_2 cross-section of the face width of the concave spherical gear can be considered as follows:

$$\mathbf{R}_{2,left} = \mathbf{R}_{2,right}, \tag{11}$$

and

$$\sqrt{X_{2,left}^2 + Y_{2,left}^2} = \sqrt{X_{2,right}^2 + Y_{2,right}^2} = r_{tl}, \tag{12}$$

where subscripts "*left*" and "*right*" of Eqs. (11) and (12) denote the left-side and right-side tooth flanks profiles of the concave spherical gear, respectively. Symbol r_{tl} of Eq. (12) indicates the radius of the tooth top circle, while symbols X_2 and Y_2 denote the X and Y components of position vector $\mathbf{R}_2$, respectively. Due to the radius of tooth top circle of the concave spherical gear is variable at every Z_2 cross section along its face width, the radius r_{tl} of Eq. (12) can be designed by $r_{tl} = r_2 + m_n + R_2(1 - \cos\theta_2)$, where term, $R_2(1 - \cos\theta_2)$, is identical to the value of profile-shifting of the concave spherical at which corresponding to the spherical angle θ_2.

4. Numerical examples

Based on the spherical gear's mathematical model and tooth undercutting conditions of the convex and concave spherical gears, the tooth flank profile deviation, tooth undercutting analysis and tooth pointing of the proposed spherical gears are investigated and illustrated by five numerical examples. It is noted that all the gears discussed in this study are external gears, and the tooth lengths of the convex and concave spherical gears at the central section of the face width are designed as a standard tooth (i.e. $a = 1.0 \times m_n$). Moreover, the major design parameters of the proposed spherical gears for these five numerical examples are all given in Table 1.

4.1. Example 1. Tooth flank profile deviations of spur, concave and convex spherical gears

Tooth flank profile deviations of convex and concave spherical gears with respect to the spur gear at different Z cross-sections (e.g. $Z = 0$ mm and $Z = \pm 7.5$ mm) can be investigated by applying the developed mathematical model of the spherical gears.

Based on the gear data given in Example 1 of Table 1, Fig. 3 shows the tooth flank profile deviations of the spur gear and spherical gears with convex and concave teeth at cross sections $Z = 0$ mm and $Z = \pm 7.5$ mm, respectively. The tooth flank profiles of Fig. 3 can be determined by utilizing Eqs. (1) and (3) and Eqs. (2) and (3) for the convex and concave spherical gears, respectively. Since there is no profile-shifting at the central section ($Z = 0$ mm) of convex and concave spherical gear teeth, the tooth flank profiles of spherical gears with convex and concave teeth at the central section are the same as that of the spur gear. Compared with the tooth flank profile of spur gears, the convex spherical gear tooth flank profile at the sections of its both ends of face width ($Z = \pm 7.5$ mm) has a shorter tooth depth and a smaller tooth thickness while the concave spherical gear has a longer tooth depth and a larger tooth thickness. It can be found that the convex spherical gear at the cross sections $Z = \pm 7.5$ mm have the smallest tooth length. If the contact position of a spherical gear pair (with a convex spherical gear) is near the cross section $Z = \pm 7.5$ mm, the contact ratio of the gear pair will decrease, however, it can be improved by increasing the spherical radius R_1 during the convex spherical gear's manufacture process.

4.2. Example 2. Investigation on the tooth undercutting of spherical gears by checking along Z_1 cross-sections

The 3-dimensional graphs of convex and concave spherical gears of Figs. 4 and 5 can be drawn by utilizing Eqs. (1) and (3) and Eqs. (2) and (3), respectively. On the tooth surfaces of Figs. 4 and 5, the mesh guild lines along the tooth profile and face width directions are the sets of surface coordinates of parameters ℓ_i and θ_j, respectively. It is noted that if a value of the Z cross-section of the face width was given as a known parameter, then parameters θ_1 and θ_2 can be defined according to the generation mechanism

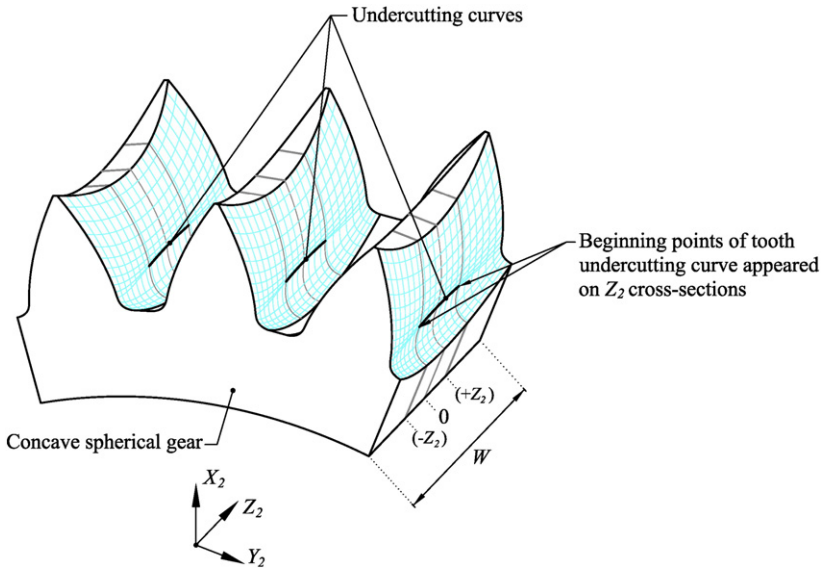

Fig. 5. Tooth undercutting of the concave spherical gear (gear data are given in Example 2 of Table 1).

of the spherical gears (Fig. 3 of literature [16]), respectively. Therefore, other unknown design parameters ℓ_i and ϕ_j can also be determined by solving Eqs. (10) and (3) for convex spherical gear ($i=F$ and $j=1$), and Eqs. (10) and (3) for concave spherical gear ($i=P$ and $j=2$). Therefore, the coordinates of singular points on the generated tooth flanks can be calculated.

Since the convex spherical gear has negative profile-shiftings at both-end sections of the gear, the occurrence of tooth undercutting of a convex spherical gear is much easier at both-end sections than other sections of the gear. According to the gear data given in Example 2 of Table 1, tooth undercutting of the convex spherical gear can be obtained as shown in Figs. 4 and 5. The value of the face width is related to the beginning points of tooth undercutting in the Z_1 cross-section (refer to Fig. 4). Since the design parameter $\ell_F = 0$ is the first position of the generated tooth profile, therefore, the position corresponding to parameter $\ell_F = 0$ is the easiest point to generate singular points on the tooth profile of the convex spherical gears. Based on the developed conditions of tooth undercutting, the cross-section along Z_1 coordinates, at which the tooth undercutting begins for a convex spherical gear, can also be calculated by considering Eqs. (10) and (3) ($i=F$ and $j=1$) with $\ell_F = 0$. Similarly, according to the gear data of the concave spherical gear given in Example 2 of Table 1, tooth undercutting curve can also be obtained as shown in Fig. 5.

4.3. Example 3. Limit curves of tooth undercutting of spherical gears on rack cutter surfaces

This example shows the positions of singular points appeared along the Z_j-axes (refer to Figs. 4 and 5) of the convex and concave spherical gears under different numbers of gear teeth. The positions of singular points are calculated and expressed in terms of the design parameters of the rack cutter. Again, a set of singular points appeared on the generated gear tooth flank which corresponds to a set of points located on rack cutter surface is called the limit curve of tooth undercutting.

Fig. 6(a) shows the locations of the singular points that appeared along the Z_1-axis of the convex spherical gear in terms of rack cutter's surface parameter ℓ_F under the conditions of pressure angle $\alpha_n = 14.5°$ and different numbers of gear teeth. The results are obtained based on the gear data given in Example 3 of Table 1. When the number of gear teeth is 31 teeth and pressure angle $\alpha_n = 14.5°$, the generated convex spherical gear at its central section of the tooth face width still has a singular point within the working interval of the design parameter ℓ_F. It means that tooth undercutting has occurred at the central section of the tooth face width for the convex spherical gear. According to the theory of gearing, the minimum tooth numbers for a spur gear without tooth undercutting under pressure angle $\alpha_n = 14.5°$ is 32 teeth.

Moreover, Fig. 6(b) shows the locations of singular points that appeared on the generated concave spherical gear in terms of the rack cutter's surface parameter ℓ_P under the pressure angle $\alpha_n = 14.5°$ with different numbers of teeth. It is noted that both end sections of the tooth face width of the concave spherical gear are positive profile-shiftings. According to the results of Fig. 6(a) and (b), it is found that a spherical gear with a larger number of teeth results in its limit curve moves to the tooth root. This result also matches the characteristics of the theory of gearing. Therefore, the analysis results shown in Fig. 6(a) and (b) are most useful for the gear designers. Moreover, it is noted that the design parameter ℓ_i has the working interval with the starting point and end point of the gear tooth flank at each Z_j ($j=1, 2$) cross-section and $\ell_{i,S} \le \ell_i \le \ell_{i,E}$ ($i=F, P$), where $\ell_{i,S} = 0.0$ mm and $\ell_{i,E} = 4.132$ mm.

4.4. Example 4. Z cross-section which tooth undercutting begins

Based on the concept of the checking of tooth undercutting, positions of the Z_j cross-section (see Figs. 4 and 5), which tooth undercutting begins, can be calculated.

Since the convex spherical gear has negative profile-shifting at both end sections of the tooth face width, the occurrence of tooth undercutting at both end sections is easier than that of the central section. Therefore, the value of the tooth face width of a convex spherical gear depends on its gear design parameters (see Fig. 4). Based on the gear data given in Example 4 of Table 1, Fig. 7 illustrates each positive Z_1 cross-section at which tooth undercutting begins for the convex spherical gear under different pressure angles and number of teeth. It is found that the proposed convex spherical gear with a smaller pressure angle (i.e. $\alpha_n = 14.5°$) should design a smaller value of the face width, and the gear with a smaller number of teeth also should design a smaller value of face width. Moreover, the value of the tooth face width is twice the value of the half face width, as shown in Fig. 7, because the proposed spherical gear is in a symmetrical profile at the cross section of $Z_1 = 0$ mm.

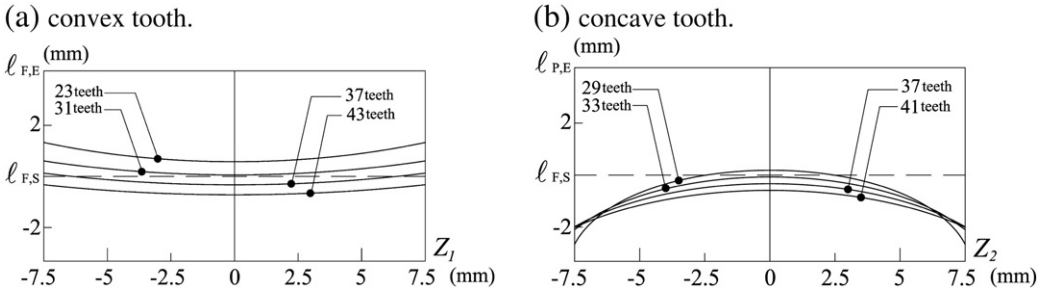

Fig. 6. Locations of limit curves of the spherical gears with the pressure angle $\alpha_n = 14.5$ (gear data are given in Example 3 of Table 1).

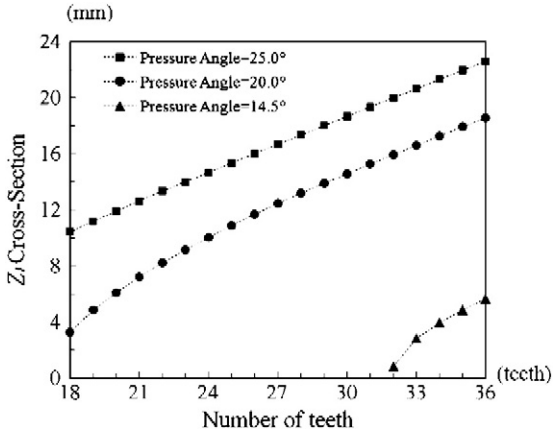

Fig. 7. Tooth undercutting begins for the spherical gears with convex tooth (gear data are given in Example 4 of Table 1).

4.5. Example 5. Z_2 cross-section which tooth pointing begins

Based on the conditions of tooth pointing of the concave spherical gear, positions of the Z_2 cross-section (see Fig. 2), which tooth pointing begins, can be calculated.

According to the data given in Example 5 of Table 1, Fig. 8(a) illustrates each positive Z_2 cross-section at which tooth pointing begins for the concave spherical gear under different pressure angles and number of teeth. It is found that to avoid tooth pointing the proposed concave spherical gear with a larger pressure angle (i.e. $\alpha_n = 25°$) should design a smaller value of the face width, and the gear with a smaller number of teeth also should design a smaller value of face width. Furthermore, Fig. 8(b) shows each positive Z_2 cross-section at which tooth pointing begins for the proposed concave spherical gear under different pressure angles and normal module. It is also found that the proposed concave spherical gear with a larger pressure angle (i.e. $\alpha_n = 25°$) should design a smaller value of the face width, and the gear with a smaller normal module also should design a smaller value of the face width. Moreover, the value of the tooth face width is twice the value of the half face width, as shown in Fig. 8, because the proposed spherical gear is in a symmetrical profile at the cross section of $Z_2 = 0$ mm.

5. Conclusions

By utilizing the proposed mathematical model of spherical gears developed in Ref. [16], the condition equations of tooth undercutting for the convex and concave spherical gears have been derived by considering the relative velocity and equation of meshing between the rack cutter and generated gear. Moreover, the tooth pointing condition equations for the concave spherical gear have also been derived. Therefore, the tooth profile variations, limit curves of tooth undercutting, and the beginning points of tooth undercutting and pointing at the Z cross-section of spherical gears were studied and verified by five numerical examples. The simulated results of this study are most helpful to the designers and manufacturers for their designs and choosing the proper

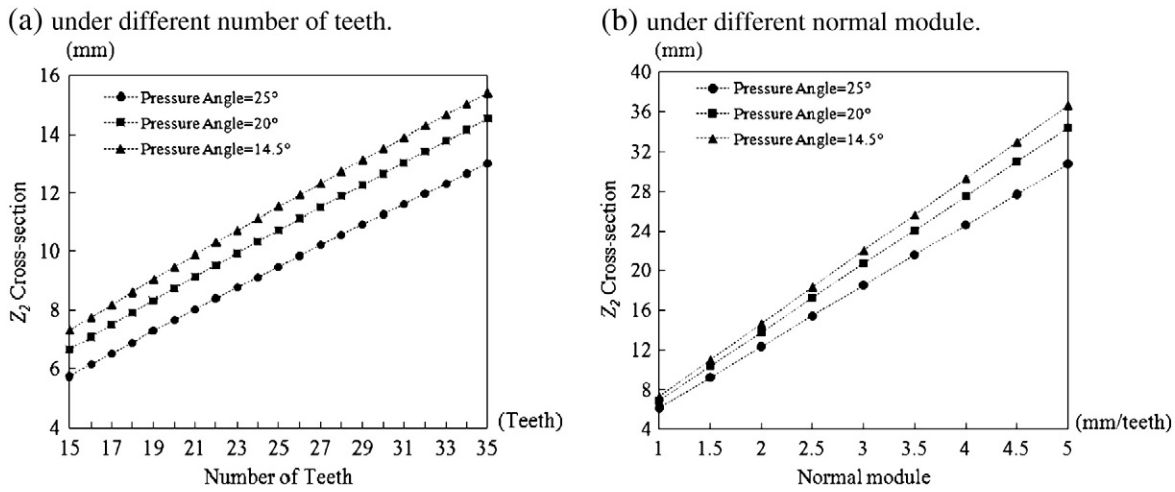

Fig. 8. Tooth pointing begins for the spherical gear with concave tooth (gear data are given in Example 5 of Table 1).

parameters for the manufacturing of spherical gears without tooth undercutting and tooth pointing. The results lead to the following conclusions:

(1) At the central section of the convex and concave spherical gears, the tooth profiles are the same as that of the spur gear, as shown in Fig. 5. Besides, the profiles at both end sections of the convex spherical gear have a shorter tooth depth and a smaller tooth thickness than those of the spur gear, whereas, the concave spherical gear has a longer tooth depth and a larger tooth thickness at its both end sections.
(2) Due to hobbing with negative profile-shiftings at both-end sections of the tooth face width, regardless of the gear teeth number, the limit curves at both ends of the convex spherical gear tend to upward, as shown in Fig. 8(a). In contrast, the concave spherical gear has both ends of its limit curves tend to downward, as shown in Fig. 8(b).
(3) For a convex spherical gear, the easiest position to occur tooth undercutting is located at both ends of the tooth face width. Whereas, the central section of the face width is the easiest position for tooth undercutting for a concave spherical gear to occur.
(4) The Z_1 cross-section, at which tooth undercutting begins, of a convex spherical gear depends on the number of teeth and pressure angle. A larger pressure angle and a larger number of teeth result in a larger value of the tooth face width. Whereas, a smaller pressure angle and a smaller number of teeth result in a smaller value of the face width.
(5) The Z_2 cross-section, at which tooth pointing begins, of a concave spherical gear depends on the pressure angle, number of teeth and normal module. A larger pressure angle, a smaller number of teeth and a smaller normal module result in a smaller value of the tooth face width.

Acknowledgements

The authors are grateful to the National Science Council of the ROC for the grant. Part of this work was performed under contract No. NSC-95-2221-E-159-002-MY3.

References

[1] DimarogonasA.D. , Machine Design: A CAD Approach, John Wiley & Sons, 2001.
[2] ChondrosT.G. , Archimedes (287–212 BC), history of mechanism and machine science 1, in: MacroCeccarelli (Ed.), Distinguished Figures in Mechanism and Machine Science, Their Contributions and Legacies Part 1, Springer, 2007, pp. 1–30.
[3] LitvinF.L. , Theory of Gearing, NASA Reference Publication 1212, Washington D. C, 1989.
[4] LitvinF.L. , FuentesA. , Gear Geometry and Applied Theory, 2nd Edition, Cambridge University Press, 2004.
[5] S.L. Chang, C.B. Tsay, L.I. Wu, Mathematical model and undercutting analysis of elliptical gears generated by rack cutters, Mechanism and Machine Theory 31 (7) (1996) 879–890.
[6] C.C. Liu, C.B. Tsay, Tooth undercutting of beveloid gears, ASME Journal of Mechanical Design 123 (4) (2001) 569–576.
[7] C.F. Chen, H.T. Lin, C.B. Tsay, Mathematical model and undercutting analysis of modified helical gears with smaller number of teeth, Journal of CSME 23 (4) (2002) 301–311.
[8] R.T. Tseng, C.B. Tsay, Mathematical model and undercutting of cylindrical gears with curvilinear shaped teeth, Mechanism and Machine Theory 36 (2001) 1189–1202.
[9] J.T. Tseng, C.B. Tsay, Mathematical model and surface deviation of cylindrical gears with curvilinear shaped teeth cut by hob cutter, ASME Journal of Mechanical Design 127 (2005) 982–987.
[10] S.C. Yang, Mathematical model of a ring-involute-teeth spherical gear with a double degree of freedom, Journal of Advanced Manufacturing Technology 20 (2002) 865–870.
[11] S.C. Yang, A rack-cutter surface used to generate a spherical gear with discrete ring-involute teeth, Journal of Advanced Manufacturing Technology 27 (2005) 14–20.
[12] S.C. Yang, Study of an elbow mechanism generated by a conical cutter, Proceeding Inst. Mechanical Engineering Part C: Journal of Mechanical Engineering Science 221 (2007) 727–738.
[13] Y.C. Tsai, W.K. Jehng, Rapid prototyping and manufacturing technology applied to the forming of spherical gear sets with skew axes, Journal of Materials Processing Technology 95 (1999) 169–179.
[14] M.L. Novikov, USSR Patent, No. 109, 750, (1956).
[15] K. Mitome, T. Okuda, T. Ohmachi, T. Yamazaki, Develop of a new hobbing of spherical gear, Journal of JSME 66 (646) (2000) 1975–1980.
[16] L.C. Chao, C.B. Tsay, Contact characteristics of spherical gears, Mechanism and Machine Theory 43 (2008) 1317–1331.